

## Transport and magnetic properties of BaVSe<sub>3</sub>

Ana Akrap,<sup>1,\*</sup> Vladan Stevanović,<sup>2</sup> Mirta Herak,<sup>3</sup> Marko Miljak,<sup>3</sup> Neven Barišić,<sup>1,4</sup> Helmuth Berger,<sup>1</sup> and László Forró<sup>1</sup>

<sup>1</sup>*Institut de Physique de la Matière Complexe, EPFL, CH-1015 Lausanne, Switzerland*

<sup>2</sup>*Institut Romand de Recherche Numérique en Physique de Matériaux (IRRMA) and Institute of Theoretical Physics (ITP),*

*Ecole Polytechnique Fédérale de Lausanne (EPFL), CH-1015 Lausanne, Switzerland*

<sup>3</sup>*Institute of Physics, P.O. Box 304, HR-10000 Zagreb, Croatia*

<sup>4</sup>*Physikalisches Institut, Universität Stuttgart, Pfaffenwaldring 57, 70550 Stuttgart, Germany*

(Received 9 September 2008; revised manuscript received 22 October 2008; published 10 December 2008)

We report a comprehensive study of transport, magnetotransport, and magnetic properties of single crystals of BaVSe<sub>3</sub>. The paramagnetic metal-ferromagnetic metal transition at 43 K was followed as a function of pressure by measuring the electrical resistivity and the thermoelectric power. The exponent of the low-temperature power-law dependence of the resistivity increases with pressure. The effective magnetic moment obtained from magnetic susceptibility in the paramagnetic regime is  $\mu_{\text{eff}} = 1.40\mu_B$ . The study was completed by band-structure calculations based on density-functional theory both at ambient and high pressures. Transport coefficients of BaVSe<sub>3</sub> resemble the high-pressure phase of BaVS<sub>3</sub>, which suggest that the replacement of sulfur with selenium can be viewed as chemical pressure.

DOI: 10.1103/PhysRevB.78.235111

PACS number(s): 74.25.Fy, 71.20.-b, 75.47.-m, 74.62.Fj

### I. INTRODUCTION

The paramagnetic-ferromagnetic (PM-FM) transition in 3d transition-metal compounds has received lot of attention because of its importance in applications, for example, in colossal magnetoresistance compounds,<sup>1</sup> or because of the exotic physics it can lead to, such as in the case of MnSi.<sup>2,3</sup> Like this latter compound, BaVSe<sub>3</sub>, which has a structurally one-dimensional character, shows a PM-metal to FM-metal transition at 43 K.<sup>4,5</sup> The in-depth investigation of this compound and its comparison to other 3d correlated systems has been precluded until now due to the lack of sizable single crystals. A further importance in studying BaVSe<sub>3</sub> is a recent interest in its sister compound of BaVS<sub>3</sub>, which has a very rich phase diagram<sup>6-8</sup> and whose high-pressure magnetic ground state is poorly understood. Formally, because of the stronger interchain overlap due to the larger selenium atoms, BaVSe<sub>3</sub> could be considered as the high-pressure counterpart of BaVS<sub>3</sub>.

The room-temperature structure of the selenide is the same as that of the sulfide and is shown in Fig. 1. Slightly above room temperature, BaVSe<sub>3</sub> crystallizes in the hexagonal  $P6_3/mmc$  symmetry.<sup>9</sup> Vanadium chains directed along  $c$  axis form a triangular lattice in the  $ab$  plane. Each vanadium atom is surrounded by a trigonally distorted octahedron of chalcogen atoms. The unit cell contains two vanadium sites along the chain. Barium atoms lay between the chains in 12 coordinated sites. Due to the difference in the chalcogen sizes, the unit cell in BaVSe<sub>3</sub> is slightly larger than in the sulfide. The V-V distance along the  $c$  direction is 2.93 Å and perpendicular to the chains is 7.0 Å. For comparison, these values are 2.8 and 6.75 Å in the sulfide. A structural transition from hexagonal to orthorhombic unit cell was reported to take place between 290 and 310 K.<sup>9</sup> This transition leads to a zigzag distortion of the vanadium chains in the  $bc$  plane.

Because of the enhanced interchain orbital overlaps, in contrast to the insulating ground state of BaVS<sub>3</sub>, the selenide was found to be metallic in the whole temperature range,<sup>4</sup>

just like BaVS<sub>3</sub> at  $p \geq 2.0$  GPa. Furthermore, it undergoes a ferromagnetic transition at  $T_c \approx 43$  K. In BaVS<sub>3</sub> under ambient pressure, magnetic order is established at  $T_X \approx 30$  K (Ref. 6): the vanadium spins order ferromagnetically along the chains, but overall the system is a helicoidal antiferromagnet.<sup>7</sup> It is not entirely clear how  $T_X$  evolves under pressure in BaVS<sub>3</sub>. The appearance of a hysteresis in the resistivity under high pressure, for  $1.75 \leq p \leq 2.0$  GPa, hints that there is possibly a crossing of the  $T_X$  and the  $T_{MI}$  in the pressure-temperature phase diagram.<sup>10</sup> In that sense, the ferromagnetic ground state of BaVSe<sub>3</sub> corroborates with the idea that this system corresponds to the high-pressure metallic phase of BaVS<sub>3</sub>.<sup>10</sup>

Although a synthesis of single crystals was reported in the original work of Kelber *et al.*,<sup>9</sup> the properties of single crystal BaVSe<sub>3</sub> have not been studied so far. All that we know about BaVSe<sub>3</sub> comes from the measurements on ceramic samples. The ferromagnetic transition could be clearly observed in such samples at ambient pressure. However, due to the polycrystallinity, the absolute value of the resistivity was unreliable. Besides, it was impossible to analyze the low-temperature functional dependence of the resistivity, which is important for comparison with the high-pressure power-law dependence of the resistivity in the metallic phase of BaVS<sub>3</sub>

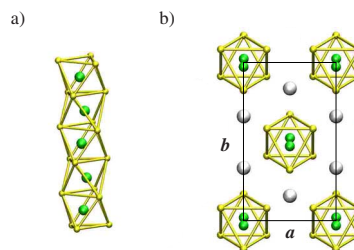


FIG. 1. (Color online) (a) A VSe<sub>3</sub> chain of BaVSe<sub>3</sub> is shown in the orthorhombic ( $Cmc2_1$ ) phase, as well as (b) the arrangement of the chains in the  $ab$  plane. Barium atoms are located in the 12 coordinated sites between the chains. In the hexagonal ( $P6_3/mmc$ ) phase vanadium atoms are aligned along the  $c$  axis and  $b = a\sqrt{3}$ .

and the transition from non-Fermi-liquid to Fermi-liquid behavior.<sup>11</sup> Furthermore, in order to ascertain the crossing of  $T_{MI}$  and  $T_X$  in the phase diagram of  $BaVS_3$ ,<sup>10</sup> it is important to investigate the behavior of  $T_c$  in  $BaVSe_3$  under pressure. When pressure is applied to ceramic samples, the main effect is the compression of grain boundaries. This leads to unreliable pressure dependence of the resistivity. It also turns out that from transport measurements done on such samples, it is difficult to extract the precise pressure dependence of the ferromagnetic transition temperature  $T_c$ .

In this paper we report a comprehensive study of magnetic and transport properties of high-quality single crystals of  $BaVSe_3$ . To compare our results with the theoretical predictions, we discuss the density-functional theory (DFT) calculations of the band structure in  $BaVSe_3$ . The main result is that in many of its properties  $BaVSe_3$  bears a strong resemblance to the high-pressure phase of  $BaVS_3$ . However, findings such as pressure enhancement of the power-law exponent  $n$  of resistivity or the pressure and magnetic-field dependence of the residual resistivity  $\rho_0$  challenge our understanding of the electrical transport at low temperatures.

## II. METHODS

Single crystals were grown using a method similar to the one described in the work of Kelber *et al.*<sup>9</sup> The crystals used in this study were in form of shiny black needles with typical dimensions of  $1 \times 0.1 \times 0.1$  mm<sup>3</sup>. The high quality of the crystals was reflected in a high residual resistivity ratio  $[(RRR)=\rho(300\text{ K})/\rho_0]$  of typically 50.

For electrical transport measurements, we used several needle-shaped crystals with typical dimensions of  $0.4 \times 0.05 \times 0.01$  mm<sup>3</sup>. A sample with four silver paint contacts was mounted on a homemade thermopower sample holder, fitting into a clamped pressure cell. Small metallic heaters installed at both ends of the sample generated the temperature gradient which was measured with a Chromel-Constantan differential thermocouple. Such a setup enabled a simultaneous measurement of the resistivity and the thermopower. The pressure medium used in this study was kerosene, and the maximum pressure attained was 2.8 GPa. The pressure was measured using a calibrated InSb pressure gauge.

Magnetic susceptibility was measured on a collection of a hundred single crystals of  $BaVSe_3$  by a Faraday method. The crystals with total mass of 4 mg were randomly placed in a sample holder. The susceptibility was measured in the temperature range from  $T_c \approx 42$  to 330 K in magnetic fields up to 0.9 T. At temperatures below  $T_c$ , field and temperature dependence of magnetization was measured by zero-field cooling.

All band-structure calculations were done using DFT. Spin-dependent generalized gradient approximation (GGA), in the Perdew-Burke-Ernzerhof (PBE) functional form,<sup>12</sup> and scalar-relativistic ultrasoft pseudopotentials are employed as implemented in the QUANTUM ESPRESSO computer package.<sup>13</sup> Electron wave functions and augmented densities are expanded in-plane waves with cutoff energies of 35 and 400 Ry, respectively. Sampling of the Brillouin zone (BZ) is

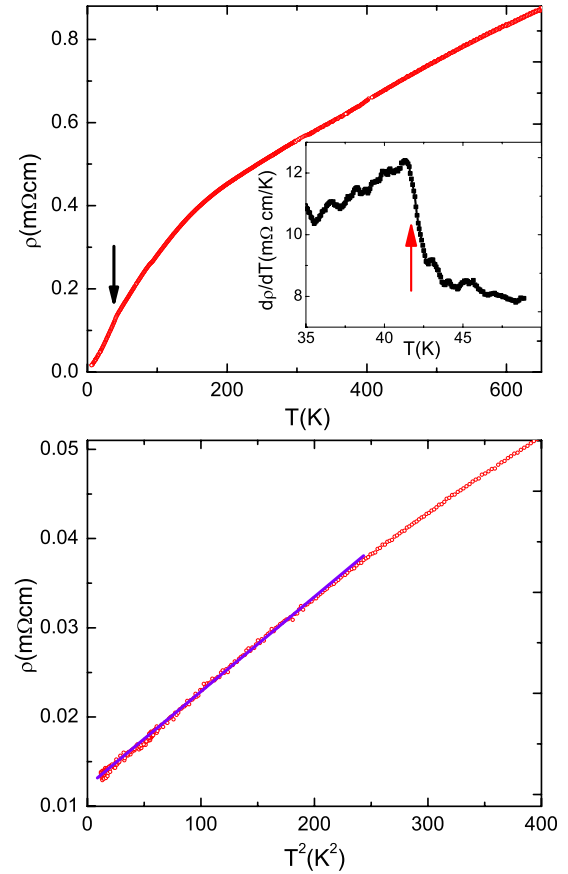


FIG. 2. (Color online) Temperature dependence of resistivity is shown in the top panel. The arrows mark the temperature of the ferromagnetic phase transition  $T_c$ , which can be better distinguished from the inset showing the derivative of the resistivity. The bottom panel demonstrates the clear  $T^2$  dependence of resistivity below 15 K.

done using  $8 \times 8 \times 8$   $\mathbf{k}$ -point grid.<sup>14</sup> Starting atomic configuration is taken from experiment and full atomic relaxation is performed in order to find an equilibrium structure. Murnaghan equation of state<sup>15</sup> is then used to find the equilibrium lattice constant. Pressures are determined by the stress tensors, which are calculated for the systems with unit cells scaled isotropically to the volumes that are 0.97 and 0.94 of the equilibrium one. Validity of this approach was tested for the last case with Parrinello-Rahman variable-cell molecular dynamics<sup>16</sup> at the constant pressure. During the simulation symmetry of the unit cell remained unchanged as well as the  $c/a$  ratio.

## III. AMBIENT PRESSURE

### A. Transport properties

The temperature dependence of the transport coefficients, resistivity, and thermoelectric power was determined at ambient pressure from 1.5 to 650 K. Given the morphology of the crystals, all the measurements were performed along the  $c$  axis. The resistivity is shown in the top panel of Fig. 2. In the previously studied ceramic samples, the room-

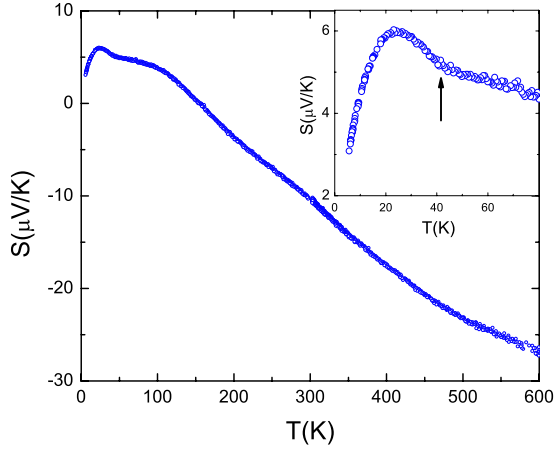


FIG. 3. (Color online) The ambient-pressure-temperature dependence of the thermoelectric power of BaVSe<sub>3</sub> is shown for temperatures up to 600 K. The inset shows a zoom on the ferromagnetic transition, and the arrow marks  $T_c$ , the temperature of the ferromagnetic ordering.

temperature value of the resistivity was approximately three times larger than the present value  $\rho_{\text{ceramics}} \sim 1.8 \text{ m}\Omega \text{ cm}$ .<sup>4</sup> The ceramic samples had a residual resistivity ratio of  $\sim 3$ , whereas for our single crystal  $\text{RRR} \approx 50$ .

The overall shape of the resistivity curve greatly resembles the high-pressure resistivity in BaVS<sub>3</sub>. At 300 K, the value of resistivity is  $0.57 \text{ m}\Omega \text{ cm}$ , which compares very well to the high-pressure value of resistivity in BaVS<sub>3</sub>,  $\rho(300 \text{ K}, 2.8 \text{ GPa}) = 0.55 \text{ m}\Omega \text{ cm}$ .<sup>11,17</sup> Such a high value of the resistivity indicates that BaVSe<sub>3</sub> is a bad metal. In the resistivity one cannot discern any signatures of a structural transition from hexagonal to orthorhombic symmetry which supposedly occurs around 300 K.<sup>9</sup> Instead, our data show that above 200 K, the resistivity is linear, indicating that the dominant mechanism in the high-temperature range is scattering on phonons. As shown in the inset of Fig. 2, an abrupt change in the slope of the resistivity appears below 42 K, where ferromagnetic ordering takes place. Below 200 K and down to  $T_c$ , the resistivity drops with a more pronounced slope, which seems to be correlated with the change in the symmetry seen by the magnetic moments.<sup>5</sup> This point will be addressed in more detail later.

The low-temperature part is particularly interesting with respect to BaVS<sub>3</sub>. Above  $p_{\text{cr}} \approx 2.0 \text{ GPa}$  the low-temperature resistivity of BaVS<sub>3</sub> may be described by a power-law temperature dependence,

$$\rho = \rho_0 + AT^n, \quad (1)$$

with  $n \approx 1.5$  in the very beginning of the metallic phase and  $n \rightarrow 2$  when the system is tuned far from  $p_{\text{cr}}$ .<sup>8,11</sup> In BaVSe<sub>3</sub>, the ambient-pressure-temperature dependence of resistivity below  $\sim 15 \text{ K}$  may be described by Eq. (1). The values of the parameters extracted from such a fit are the following:  $\rho_0 = 12.9 \mu\Omega \text{ cm}$ ,  $A = 1.16 \times 10^{-4} \text{ m}\Omega \text{ cm}$ , and  $n = 2.00 \pm 0.01$ . Indeed, a clear  $T^2$  dependence may be seen from the lower panel of Fig. 2.

Figure 3 shows the temperature dependence of thermo-

electric power in BaVSe<sub>3</sub>. Again, the shape of the curve is qualitatively very similar to the high-pressure phase of BaVS<sub>3</sub>.<sup>18</sup> The high-temperature part of the curve ( $100 \text{ K} < T < 500 \text{ K}$ ) is linear, just as it is expected in a metal. The high absolute value of this transport coefficient confirms the bad metallicity of BaVSe<sub>3</sub>. To obtain an estimate of the value of Fermi energy  $E_F$ , we may apply the formula describing the thermopower of a free-electron gas with an energy-independent scattering rate,<sup>19</sup>

$$S = -\frac{\pi^2 k_B^2 T}{2|e|E_F}. \quad (2)$$

This gives  $E_F \approx 0.52 \text{ eV}$ . However, the thermopower of BaVSe<sub>3</sub> has a significant offset  $11.2 \mu\text{V/K}$  instead of extrapolating into zero for  $T=0$  as the above Mott formula would predict. The origin of this temperature-independent contribution may be polaronic or might be more general, which has so far not been discussed in the literature.<sup>20</sup> Apart from the high-temperature linear behavior, thermopower displays a wide hump centered around 100 K and a low-temperature maximum at  $\sim 20 \text{ K}$ . The corresponding low-temperature maximum in BaVS<sub>3</sub> under high pressure  $p > p_{\text{cr}}$  has been attributed to phonon drag.<sup>18</sup> However, this local maximum in BaVS<sub>3</sub> has a strong magnetic-field dependence, which suggests that there may also be a magnon contribution present.

Besides the qualitative similarity of the sulfide and the selenide resistivity curves, the fact that their thermopower is also very similar firmly establishes BaVSe<sub>3</sub> as a high-pressure counterpart of BaVS<sub>3</sub>. The high-temperature part of the high-pressure phase of BaVS<sub>3</sub> is presently experimentally inaccessible since the clamped pressure cell which has been employed so far cannot be heated above 350 K. Measuring BaVSe<sub>3</sub> is in this sense also interesting because it indicates what sort of temperature dependence of the transport coefficients is expected up to 650 K in the sulfide compound under  $\sim 3 \text{ GPa}$ .

## B. Magnetization and susceptibility

Figure 4 shows the temperature dependence of inverse magnetic susceptibility,  $1/\chi$ , in the paramagnetic regime from 43 to 330 K. We note that neither in this property can a structural transition be discerned in the vicinity of 300 K. Paramagnetic susceptibility obeys Curie-Weiss law  $\chi = C/(T - \Theta)$ , practically in the entire temperature range. The fit to Curie-Weiss plot  $1/\chi = T/C - \Theta/C$  gives the following values for Curie constant  $C$  and Curie-Weiss temperature  $\Theta$ :  $C = 0.244 \text{ emu K/mol}$  and  $\Theta = +44 \text{ K}$ . Positive  $\Theta$  signifies ferromagnetic interaction of spins which results in ferromagnetic ordering below 43 K. Effective magnetic moment obtained from Curie constant in the paramagnetic regime is  $\mu_{\text{eff}} = 1.40 \mu_B/\text{f.u.}$  Effective magnetic moment reported previously is slightly larger,  $1.42 \mu_B$ .<sup>4</sup> The reason for this discrepancy is that the authors subtracted the temperature-independent diamagnetism  $\chi_{\text{dia}} = -1.5 \times 10^4 \text{ emu/mol}$ , thus increasing the value of susceptibility. To fully incorporate the temperature-independent part of susceptibility, the Van Vleck paramagnetic susceptibility should also be subtracted. The

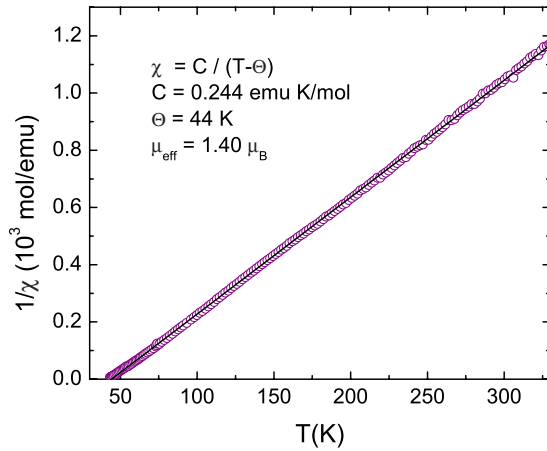


FIG. 4. (Color online) Temperature dependence of the inverse magnetic susceptibility of BaVSe<sub>3</sub>.

value of this contribution is usually  $\approx 10^{-4}$  emu/mol, so that diamagnetic and paramagnetic temperature-independent susceptibilities nearly cancel. This is why here Curie-Weiss fit was done on measured susceptibility without subtracting any temperature-independent parts. The effective moment is somewhat higher than the ambient-pressure value in the paramagnetic phase of BaVS<sub>3</sub>,  $\mu_{\text{eff}} = 1.2\mu_B$ .

Below 43 K magnetization increases rapidly with decreasing temperature. Figure 5 shows temperature dependence of  $M/H$  measured in several different fields ranging from 0.02 to 0.12 T. Figure 6 shows field dependence of magnetization at several different temperatures below  $T_c$ . In both cases, the sample was cooled below  $T_c$  in zero field. Magnetization displays saturating behavior after a very rapid increase in low fields ( $H < 0.1$  T). Similar field dependence was also observed in Ref. 4. As can be seen from Fig. 5,  $M/H$  at certain temperature is larger for smaller fields, which is the effect of the rapidly saturating behavior of the magnetization shown in Fig. 6. This is the reason why  $M/H$  measured here

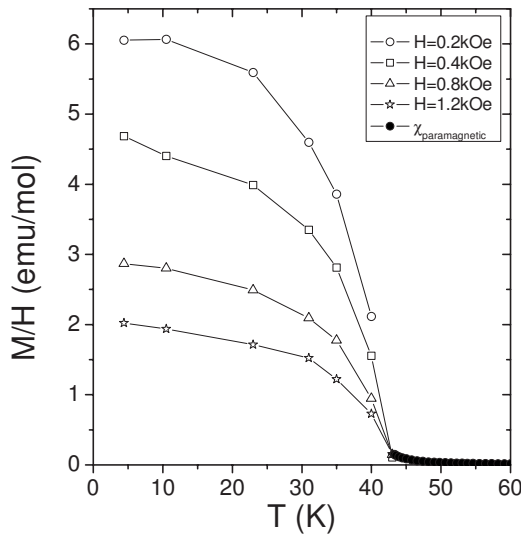


FIG. 5. Temperature dependence of  $M/H$  at several different fields below  $T_c$ . Also shown is paramagnetic susceptibility above  $T_c$ .

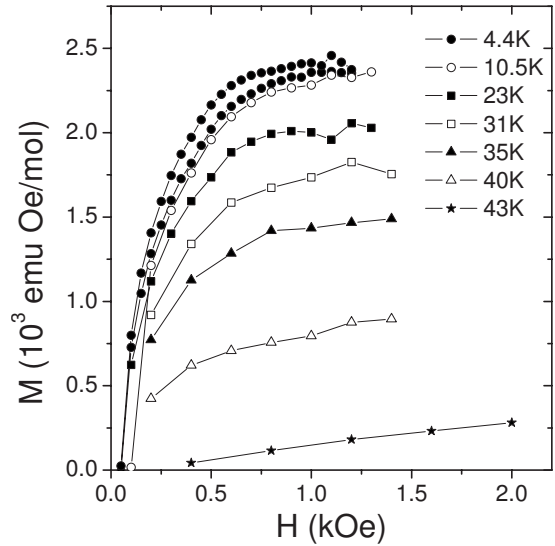


FIG. 6. Field dependence of magnetization  $M$  at several different temperatures below  $T_c$ .

in small fields is almost 2 orders of magnitude larger than the one shown in Ref. 4, where the applied field was 1 T compared to 0.12 T in our case. Also shown in Fig. 5 is the paramagnetic susceptibility of BaVSe<sub>3</sub> in the temperature range  $43 < T < 60$  K.

The properties of the ferromagnetic phase below  $T_c$  were also investigated by means of torque magnetometry and the measurement of susceptibility anisotropy, as reported by Herak *et al.*<sup>5</sup> The angular dependence of torque in the magnetic field disclosed that the system is a ferromagnet with uniaxial polarization. The absolute value of the torque determined at 4.2 K was found to be about 20 times higher when the magnetic field is directed parallel to the  $c$  axis than in the orthogonal configuration. In the case of a uniaxial ferromagnet, this implies that the large component of the magnetic moment is oriented along the  $c$  axis, which contrasts the theoretical predictions based on group theory and symmetry arguments, claiming that the large component is in the  $ab$  plane.<sup>21</sup> The torque measurement also allowed us to determine the effective moment of the ferromagnetic phase, giving  $\mu_{\text{eff}} = (0.6 \pm 0.2)\mu_B$  per vanadium atom.<sup>5</sup> The correlation between the magnetic susceptibility and the torque in the paramagnetic phase implies that below 200 K, the magnetic moments experience a changing symmetry. Interestingly, this is precisely the temperature below which the resistivity starts decreasing with a larger slope.

#### IV. BAND-STRUCTURE CALCULATIONS

In order to compare the experimental results obtained for the BaVSe<sub>3</sub> single crystals with the theoretical predictions, the DFT-based band-structure calculations were performed. Since the DFT is a ground-state theory, it is reasonable to compare quantitatively only those experimental results which reflect the ground-state properties.

Calculations of the lattice constant in the hexagonal phase agree well with experimental results. Calculated values for

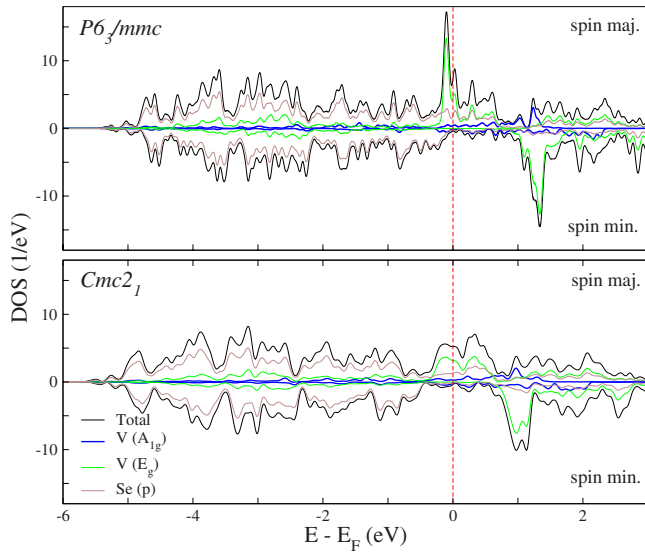


FIG. 7. (Color online) Spin-resolved DOS, in the region around the Fermi energy, is shown for  $P6_3/mmc$  and  $Cmc2_1$  BaVSe<sub>3</sub> crystal structures. Projections on the vanadium  $A_{1g}$  and  $E_g$  and the Se  $4p$  orbitals are also shown.

$a=7.01$  Å and  $c=5.87$  Å differ only by 0.15% from those reported in experiments:  $a=6.9990(11)$  Å and  $c=5.8621(13)$  Å.<sup>9,22</sup> Measurements show that slightly above the room-temperature crystal structure of BaVSe<sub>3</sub> belongs to the  $P6_3/mmc$  symmetry, while it is not clear what happens at lower temperatures. Some notions that BaVSe<sub>3</sub> undergo, similarly to the sulfide, a phase transition to the orthorhombic structure somewhere between 290 and 310 K exists in the literature; but measured values of the lattice parameters for this phase are not, to our knowledge, available in the literature. Kelber *et al.*<sup>9</sup> speculated about orthorhombic phase of BaVSe<sub>3</sub>, but they reported only the structural parameters for the hexagonal one. On the other hand Poulsen<sup>22</sup> has found that at room temperature BaVSe<sub>3</sub> becomes orthorhombic when some of barium is replaced by a small amount of potassium. In order to clarify the issue of the structure, we carried out a set of calculations and found that—as in the case of the sulfide—the phase with the  $Cmc2_1$  symmetry indeed has a lower total energy than the hexagonal one for about 0.1 eV/f.u. Calculated lattice parameters in the orthorhombic phase are  $a=7.06$  Å,  $b=12.00$  Å, and  $c=5.85$  Å.<sup>23</sup> Vanadium atoms are no longer aligned along the  $c$  axis but are displaced in the  $b$  direction forming a zigzag chain (see Fig. 1). In both phases the unit cell contains two vanadium atoms which are equivalent by symmetry and therefore no gap is opened.

We also find that the bulk modulus at the equilibrium volume differs considerably for the two phases. The value of 62 GPa in the orthorhombic phase is almost double compared to the one in the hexagonal phase (38 GPa) indicating that the low-temperature structure is much less sensitive to external pressure.

Theoretical results for the electronic ground state agree both qualitatively and quantitatively with the experiments. As shown in Fig. 7, where the spin-resolved density of states (DOS) is presented for both phases, the system is correctly

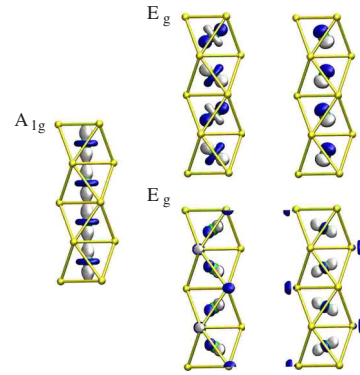


FIG. 8. (Color online) VSe<sub>3</sub> chains are shown together with the  $A_{1g}$  and  $E_g$  electronic states of the hexagonal BaVSe<sub>3</sub> at the  $\Gamma$  point in the Brillouin zone. The  $A_{1g}$  and  $E_g$  orbitals coming from the splitting of the  $T_{1g}$  triplet do not interact with the Se  $4p$  orbitals, while there is some mixing of the second  $E_g$  doublet and the Se orbitals.

predicted to be metallic and ferromagnetic. Vanadium  $d$  orbitals split in the octahedral field into the  $T_{2g}$  and  $E_g$  multiplets. By forming the chains and placing them into the  $P6_3/mmc$  structure, the octahedral symmetry is broken and the  $T_{2g}$  triplet splits into the  $A_{1g}$  singlet and  $E_g$  doublet. The  $A_{1g}$  orbitals are able to interact along the chains and form nearly quasi-one-dimensional band. On the other hand, the orbitals from the  $E_g$  doublet do not interact appreciably with their environment and therefore they form almost dispersionless bands which are responsible for the sharp peak structure of DOS just below the Fermi energy. Interaction of the atomic orbitals from the second  $E_g$  doublet with  $4p$  orbitals of the neighboring Se atoms is stronger and is responsible for the formation of bands which are located further below and above the Fermi energy. Figure 8 shows the electronic states formed by the vanadium  $A_{1g}$  and  $E_g$  orbitals at the  $\Gamma$  point of the hexagonal Brillouin zone. The states are labeled according to the irreducible representations of the corresponding crystal point group ( $D_{3h}$ ).<sup>24</sup> Two types of  $E_g$  states are shown. The first one is entirely composed of the vanadium  $E_g$  orbitals and the other one mixes with the selenium  $p$  orbitals.  $E_g$  states which have nonzero projection on the orbitals of the selenium atoms are positioned about 2 eV below the Fermi energy, while the states constituted out of the  $E_g$  orbitals coming from the  $T_{2g}$  splitting lay only 0.12 eV below the Fermi energy.

In the octahedral phase the hexagonal symmetry is broken and the vanadium  $E_g$  doublets split in the crystal field. This enhances the mixing with the selenium orbitals and the sharp peak structure in the DOS is smeared out. Mixing is stronger in the spin-majority channel due to the smaller energy difference compared to the selenium  $p$  bands. The effect of the symmetry breaking can also be seen in the band structures of these two BaVSe<sub>3</sub> phases as shown in Fig. 9. Flat doubly degenerate bands near the Fermi energy in the hexagonal phase split due to the lower symmetry of the orthorhombic phase into nondegenerate bands whose bandwidth increases. In both phases, the glide planes in the direction of the chains exist (mirror symmetry in the  $ac$  plane combined with the half-period translation) and the translational period along the

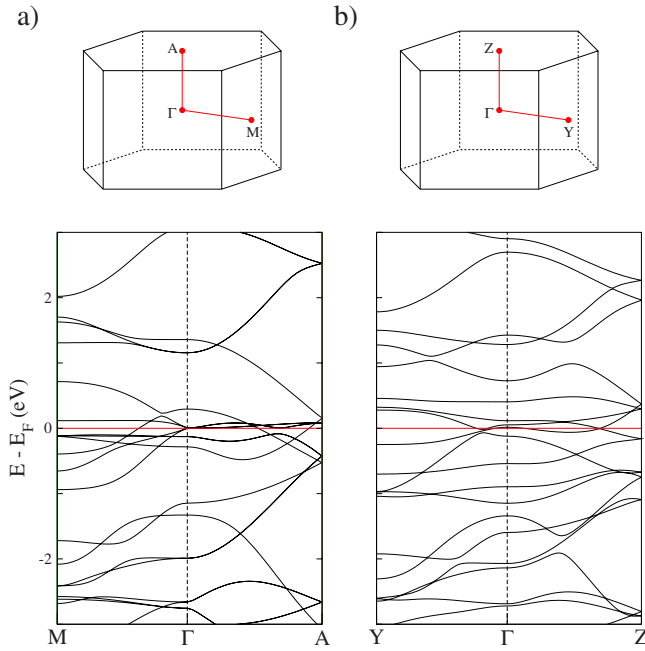


FIG. 9. (Color online) The Brillouin zone and the spin-majority band structure along the high-symmetry directions of the (a) hexagonal and (b) orthorhombic BaVSe<sub>3</sub> crystal structures.

chains contains two full symmetry elementary units (symcells<sup>25</sup>). Therefore, the folded structure of the bands can clearly be seen along the  $\Gamma$ -A and  $\Gamma$ -Z directions of both  $P6_3/mmc$  and  $Cmc2_1$  phases, respectively.

In Refs. 26 and 27 Lechermann *et al.* showed that the filling of the vanadium  $A_{1g}$  and  $E_g$  orbitals in the case of sulfide compound is not correctly predicted by DFT methods. They prove that results obtained in the local-density approximation (LDA) to DFT need to be corrected by the dynamical mean-field theory (DMFT), which includes the effects of strong correlations, in order to come closer to the understanding of the metal to insulator phase transition in BaVS<sub>3</sub>. Otherwise the filling of the vanadium  $A_{1g}$  ( $E_g$ ) orbitals is overestimated (underestimated) and the LDA picture does not provide a Fermi-surface nesting needed for the charge-density wave instability. However, qualitative LDA picture of both phases, which predicts that the low-energy sector is almost completely determined by the vanadium  $d$  bands, remains valid. Our GGA band structure of the sulfide is similar to the one obtained within the LDA approximation. In the case of selenide compound we find that bigger dispersion of the  $p$  bands caused by the size difference between S and Se ions leads to the appearance of a purely selenium band which cuts the Fermi surface. In Fig. 10 band structure of the hexagonal BaVSe<sub>3</sub> along the  $\Gamma$ -A direction is shown together with the corresponding DOS. Three types of bands that determine low-energy behavior of BaVSe<sub>3</sub> can be clearly distinguished: the nearly dispersionless  $E$  bands, quasi-one-dimensional  $A_1$  band formed by the vanadium  $A_{1g}$  orbitals, and  $A_2$  band formed exclusively of selenium  $4p$  orbitals. In the case of BaVS<sub>3</sub> the  $A_2$  band lays completely below the Fermi energy. Therefore, the low-energy sector of BaVSe<sub>3</sub> compound has more of the selenium  $p$  and less  $E_g$  character than the corresponding energy sector of the sulfide.

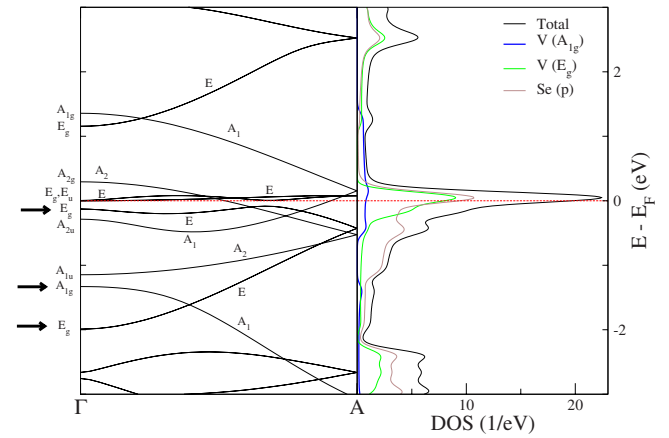


FIG. 10. (Color online) Electronic bands along the  $c$  axis together with the corresponding DOS. Bands are labeled according to the symmetry properties of the  $\Gamma$  point and  $\Gamma$ -A direction (see text). Arrows indicate the states at  $\Gamma$  which are shown in Fig. 8.

This influences the filling of vanadium  $d$  orbitals and may stabilize the orthorhombic phase as it is seen in experiments.

In the spin minority channel,  $E_g$  bands are shifted above Fermi surface due to exchange interaction leading to nonzero magnetic moment which is localized around vanadium atoms and amounts to  $1.63\mu_B$  per unit cell in the orthorhombic phase. This gives a moment of  $0.82\mu_B$  per vanadium atom, which is a reasonable value in comparison with the experimental result for the ferromagnetic phase  $(0.6 \pm 0.2)\mu_B$ .<sup>5</sup>

For the high-pressure transport measurements which follow, it is important to consider the changes in the band structure upon applying pressure. The method which was used gave no dramatic changes. At pressures lower than 3 GPa, the lattice parameters of the orthorhombic phase are expected to change not more than 2% which does not affect the electronic ground state considerably. As expected, the orbitals overlap more and the spectra broaden. In Fig. 11, DOS of two groups of bands of the orthorhombic BaVSe<sub>3</sub> is shown as well as how it changes with applied pressure. The first group located at the energies between  $-15$  and  $-10$  eV be-

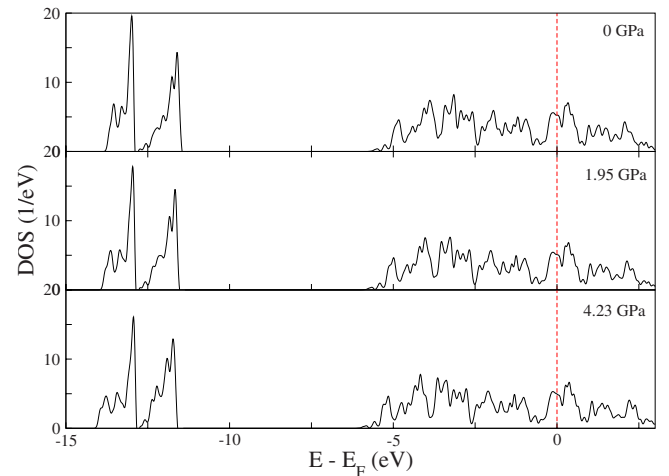


FIG. 11. (Color online) Spin-majority DOS of the orthorhombic BaVSe<sub>3</sub> at different pressures is shown.

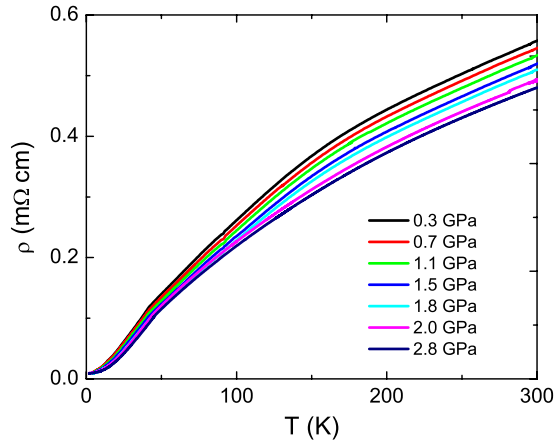


FIG. 12. (Color online) The temperature dependence of resistivity under various pressures.

low the Fermi energy consists of barium  $5p$  and selenium  $4s$  orbitals. Their interaction is enhanced and the DOS broadens with the pressure. The same occurs with the second group of bands located around the Fermi energy and formed by vanadium  $3d$  and selenium  $4p$  orbitals. It is evident that the broadening, although quite small, occurs mainly in the low-energy sector (below  $-2.5$  eV) within the selenium  $p$  bands. On the other hand, the structure of the DOS in the vicinity of the Fermi energy almost does not change up to the pressure of 4.23 GPa. We also find that the magnetic moment decreases only slightly upon applying pressure from the value of  $0.82\mu_B$  at zero pressure to the  $0.79\mu_B$  and  $0.73\mu_B$  at 1.95 and 4.23 GPa, respectively.

### V. HIGH-PRESSURE TRANSPORT PROPERTIES

The metal-insulator transition in BaVS<sub>3</sub> or the PM-FM transition in MnSi exhibits a remarkable sensitivity to pressure.<sup>8,10,11,28</sup> In both systems moderate pressures of 1.5–2.0 GPa drive the system into a non-Fermi-liquid state. This was the prime motivation to investigate BaVSe<sub>3</sub> under hydrostatic pressure. Furthermore, since BaVSe<sub>3</sub> at ambient pressure resembles to BaVS<sub>3</sub> at  $\sim 3$  GPa, it could give a hint how the latter compound would evolve at even higher pressures.

Figure 12 displays the temperature dependence of resistivity of BaVSe<sub>3</sub> under high pressures up to 2.8 GPa. The value of resistivity monotonously decreases as pressure is applied and by 2.8 GPa its room-temperature value has dropped by more than 20%. The resistivity of metals is normally reduced under pressure due to the effects of enhanced bandwidth and/or because the relaxation time  $\tau$  becomes longer. The RRR value in BaVSe<sub>3</sub> increases from 50 at ambient pressure to 55 under 2.8 GPa, which implies that the relative change in  $\rho_0$  is larger than in  $\rho(300$  K). Like in BaVS<sub>3</sub>, such pressure dependence of  $\rho_0$  hints that this quantity may contain other contributions apart from impurity scattering.

From the position of the kink in the resistivity measurements, one may extract the pressure dependence of the temperature of the ferromagnetic ordering  $T_c$ , which is shown in

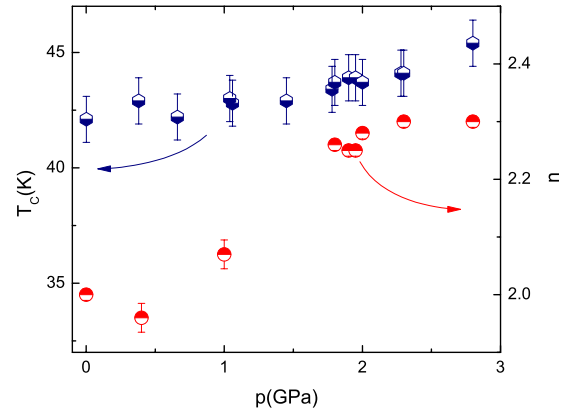


FIG. 13. (Color online) The pressure dependence of the temperature of magnetic ordering  $T_c$  (left scale) and of the resistivity exponent  $n$  (right scale).

Fig. 13. There seems to be a weak increase in  $T_c$  at a rate of  $\sim 0.9$  K/GPa. This indicates that the pressure strengthens the ferromagnetic interaction between the localized moments. The increase in  $T_c$  in BaVSe<sub>3</sub> is at variance with the behavior of the low-pressure insulating phase of BaVS<sub>3</sub>, where a feeble decrease in  $T_X$  up to  $\sim 0.5$  GPa was observed.<sup>29</sup> However, both the decrease in  $T_X$  in BaVS<sub>3</sub> and the increase in  $T_c$  in BaVSe<sub>3</sub> are unified in the phase diagram of Ba<sub>1-x</sub>Sr<sub>x</sub>VS<sub>3</sub>, where a part of barium atoms is substituted by smaller but isovalent strontium atoms.<sup>30</sup> Because of the size differences between barium and strontium atoms, increasing the strontium content  $x$  causes a decrease in the interchain spacing and thus leads to an effective chemical pressure. As  $x$  grows from 0 to 0.07, the antiferromagnetic transition is slowly suppressed, just as it happens in the pure BaVS<sub>3</sub> under hydrostatic pressure. At  $x_{cr}=0.07$ , the unit cell suddenly shrinks and the antiferromagnetic ground state gives way to ferromagnetism. When the strontium content  $x$  increases from  $x_{cr}$  until the solubility limit  $x \approx 0.18$ , the temperature of the ferromagnetic transition shows a weak increase, which may be compared to our present observations on BaVSe<sub>3</sub> under hydrostatic pressure.

In the  $3d$  transition-metal compound MnSi, the ferromagnetic metallic phase collapses under a moderate pressure of 1.5 GPa and the power-law exponent of the resistivity changes from  $n=2$  to a non-Fermi-liquid value of 1.5.<sup>28</sup> In BaVSe<sub>3</sub>, pressure also influences the resistivity coefficient  $n$  describing the power-law behavior of the resistivity below  $\sim 15$  K according to Eq. (1), but in a surprisingly different way. The evolution of  $n$  under pressure is shown in Fig. 13. Upon the application of pressure the exponent  $n$  is enhanced beyond its Fermi-liquid value of  $n=2$  and reaches the value of 2.3 under 2.8 GPa, the maximum applied pressure. It is possible that the increase in exponent continues under higher pressures toward the next meaningful exponent 3. A plausible interpretation of the observed increase in  $n$  is that the pressure reduces the temperature range where electron-electron scattering dominates and makes some other scattering mechanism, for instance, electron-phonon interaction, shows up through the exponent  $n$ .

One additional reason for unclarity regarding the origin of a low-temperature exponent  $2 < n < 3$  is the phonon-drag ef-

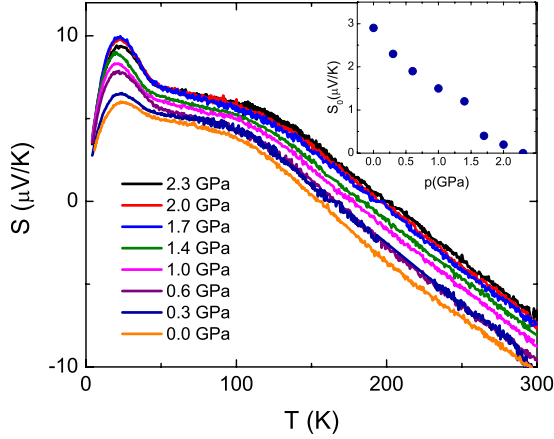


FIG. 14. (Color online) Temperature dependence of thermoelectric power under various pressures. The inset shows the offset  $S_0$ , as discussed in the text.

fect which can further suppress resistivity by pulling the phonon distribution off equilibrium.<sup>31</sup> At low temperatures, electron-phonon scattering produces quasiparticle relaxation rates going as  $T^3$ . This term in the resistivity is suppressed because the scattering is mainly restricted to small angles, which results in Bloch's  $T^5$  dependence of the electron-phonon contribution to resistivity. However, in 1935, Mott<sup>32</sup> suggested a somewhat naive  $sd$  model in which there are two types of valence electrons: nearly free  $s$  electrons and tightly bound  $d$  electrons. He assumed that the transport arises from the motion of the  $s$  electrons and that the current is primarily limited by their scattering into  $d$  states. In his model, large-angle scattering was allowed at fairly low temperatures, leading to a possible  $T^3$  dependence of the resistivity for electron-phonon scattering. Since then several calculations have been performed on magnetic systems, both ferromagnetic<sup>33</sup> and antiferromagnetic,<sup>34</sup> and it has become quantitatively clear that electron scattering on spin waves influences the power law of the temperature dependence of the low-temperature resistivity. It is reasonable to expect that pressure stiffens the ferromagnetic order which could alter the electron-magnon scattering and could lead to power-law behavior such as what we observe in BaVSe<sub>3</sub> under high pressure.

The thermoelectric power under pressure is shown in Fig. 14. The slope of the linear part appears not to be significantly influenced by pressure. This means according to Eq. (2) that the value of  $E_F$  remains unchanged. Therefore, the pressure does not influence the bandwidth. Combining this result with the observed resistivity decrease, we may conclude that the primary effect of the pressure is enhancing the relaxation time  $\tau$ . Such a conclusion is coherent with the fact that thermopower is independent of  $\tau$  in the first approximation, where the energy dependence of the relaxation time is neglected. It is also consistent with the band-structure calculations, which suggest very little pressure dependence of the DOS at the Fermi level.

On the contrary, the temperature-independent offset is increased under pressure by more than 3  $\mu\text{V}/\text{K}$ , as shown in the inset of Fig. 14. We define  $S_0$  for a given pressure as the offset of the linear part of thermopower with respect to the highest-pressure thermopower,

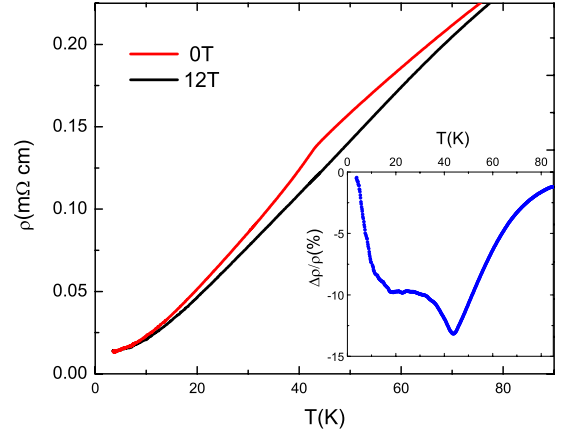


FIG. 15. (Color online) Ambient-pressure resistivity at 0 and 12 T. The magnetic field is directed along the VSe<sub>3</sub> chains,  $B \parallel c$  axis. Inset shows the relative magnetoresistance,  $\Delta\rho/\rho$ , as defined in the text.

$$S_0(p) = S(2.3 \text{ GPa}, T) - S(p, T),$$

where  $150 \text{ K} < T < 300 \text{ K}$ . In BaVS<sub>3</sub>,  $S_0$  changes by 14  $\mu\text{V}/\text{K}$  under 2.7 GPa.<sup>18</sup> In BaVSe<sub>3</sub> the change in  $S_0$  is smaller, but the trend is continued. The existence of such an offset in thermoelectric power is nontrivial to understand. As mentioned earlier, one possibility is that its origin is polaronic. In that case, as the pressure improves the metallicity of the system, the polaronic contribution should diminish and  $S_0$  should eventually converge to a pressure-independent value.

The wide hump which appears around 100 K in the thermopower at ambient pressure shifts to slightly higher temperatures when pressure is applied at an approximate rate of 7 K/GPa. This suggests that the feature may have a phononic origin. The increase in the characteristic temperature would in that case come from the pressure-induced stiffening of the relevant vibrational modes. Finally, the low-temperature feature ascribed to phonon drag becomes more pronounced under pressure but the temperature of the maximum value shows no pressure dependence.

## VI. MAGNETOTRANSPORT

Due to its ferromagnetic ground state, the transport properties of BaVSe<sub>3</sub> are expected to be fairly sensitive to an external magnetic field. Figure 15 shows a comparison between the resistivity measured in zero field and the one measured in magnetic field  $B = 12 \text{ T}$  oriented parallel to the crystal  $c$  axis. Indeed, there is a large response of the carrier scattering to the applied field. The slope change at  $T_c$  associated with the magnetic transition is completely wiped out in the magnetic field. To quantify magnetoresistance, we employ the usual definition

$$\frac{\Delta\rho}{\rho} = \frac{\rho(B) - \rho_{0 \text{ T}}}{\rho_{0 \text{ T}}}, \quad (3)$$

where  $\rho_{0 \text{ T}}$  is the zero-field resistivity. The temperature dependence of  $\Delta\rho/\rho$  is shown in the inset of Fig. 15. At high

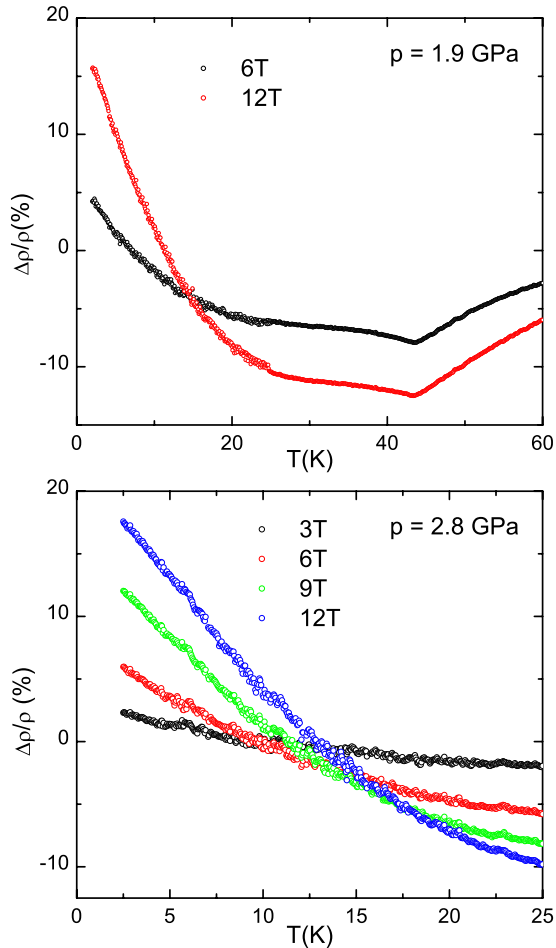


FIG. 16. (Color online) High-pressure-temperature dependence of magnetoresistance at 1.9 and 2.8 GPa. The magnetic-field orientation is  $B \perp c$  axis.

temperatures, above  $\sim 120$  K, the magnetoresistance vanishes. The negative  $\Delta\rho/\rho$  below this temperature is attributed to the ordering of magnetic moments by the external field. Magnetic field suppresses spin fluctuations and in this way decreases scattering in the conduction electrons on the magnetic moments. The extremum value of magnetoresistivity amounts to  $\sim -13\%$  and occurs precisely at  $T_c$ . Below 10 K the magnetoresistance starts to increase steeply.

Similar behavior of the resistivity is observed when pressure is applied and if the direction of the magnetic field is changed. Figure 16 shows the temperature dependence of magnetoresistance under two different high pressures, 1.9 and 2.8 GPa, in a field orientation such that  $B$  is perpendicular to the  $c$  axis. The high-temperature behavior of  $\Delta\rho/\rho$  at 1.9 GPa (top panel) is similar to the ambient-pressure dependence from Fig. 15. However, the peak at  $T_c$  is somewhat less pronounced. This seems to be correlated with the weakening of the signature of the ferromagnetic transition in resistivity. In the low-temperature part, magnetoresistance changes the sign at  $\sim 12$  K for the field  $B=12$  T. Under 2.8 GPa, the maximum value of magnetoresistance approaches 20% for the maximal magnetic field applied (Fig. 16, bottom panel).

In an ordinary paramagnetic metal, the magnetoresistance is negative in the temperature region where the external field

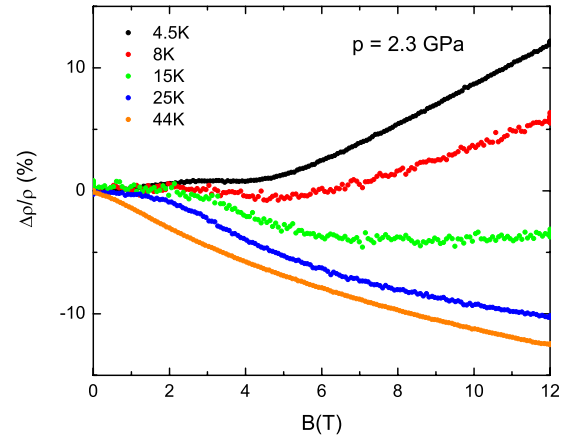


FIG. 17. (Color online) The field dependence of magnetoresistance at 2.3 GPa at several temperatures. The field is perpendicular to VSe<sub>3</sub> chains,  $B \perp c$  axis.

can align magnetic moments and thus reduce the scattering of the conduction electrons off these moments. At low temperatures, the magnetic moments in BaVSe<sub>3</sub> are more aligned and fluctuate less, which is why the field has little additional effect on their ordering. Hence, a positive magnetoresistance takes over, characteristic of normal metals.

In BaVS<sub>3</sub> the field dependence of the resistivity is a non-monotonous function.<sup>10</sup> To establish whether such behavior extends to BaVSe<sub>3</sub>, we have determined the field dependence of the magnetoresistance at several fixed temperatures for  $p=2.3$  GPa and  $B$  perpendicular to  $c$  axis. Figure 17 displays the results. The magnetoresistance changes character between 8 and 15 K, in agreement with the data discussed above: at high temperatures it is negative, whereas for low temperatures it becomes positive. Notably, at 4.5 K a small local maximum appears at  $B \sim 3$  T, after which magnetoresistance decreases slightly, and then increases linearly above  $B \sim 5$  T. A feature of similar shape in magnetoresistance may still be seen at 25 K, but for  $T=44$  K there is no trace of a local maximum, only a monotonous decrease in the whole field range. A comparable distinction between the low- and high-temperature behaviors of magnetoresistance was also observed in BaVS<sub>3</sub> at pressures above  $\sim 2.1$  GPa.<sup>11</sup> The temperature where the character of magnetoresistivity changes was also found to be rather close to what we observe here, namely, in the range between 8 and 15 K. However, the local maximum at low temperatures in BaVS<sub>3</sub> is much more pronounced. In BaVS<sub>3</sub>, it can be argued that the nonmonotonous field dependence of the resistivity comes from the canting of the  $E_g$  spins and their strong interaction with the  $A_{1g}$  electrons. This explanation may also be applied to BaVSe<sub>3</sub>, providing another point of comparison between the selenide and the sulfide.

Finally, Fig. 18 illustrates the pressure and magnetic-field dependence of coefficient  $\rho_0$  which describes the zero-temperature extrapolation of resistivity. Residual resistivity  $\rho_0$  is monotonously diminished under pressure. In a normal metal,  $\rho_0$  bears no great importance, as it is merely a measure of the impurity concentration. However, in BaVS<sub>3</sub> and BaVSe<sub>3</sub> its origin is certainly not so simple. The pressure dependence of  $\rho_0$  in BaVS<sub>3</sub> is anomalous: a sharp decrease in

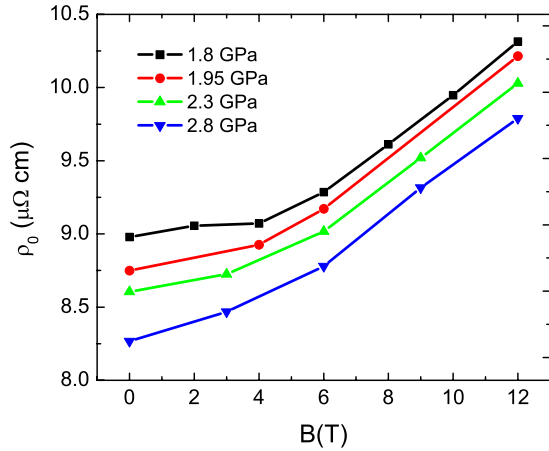


FIG. 18. (Color online) Pressure and magnetic-field ( $B \perp c$  axis) dependence of the residual resistivity  $\rho_0$ .

$\rho_0$  occurs simultaneously with the tuning of the power-law coefficient  $n$  toward the Fermi-liquid value.<sup>11</sup> This may be explained by the fact that close to the pressure where the insulating phase is suppressed, both  $n$  and  $\rho_0$  issue from the scattering of conduction electrons on the charge fluctuations in the  $A_{1g}$  sector. When pressure is increased toward 3 GPa,  $\text{BaVS}_3$  approaches the  $n=2$  value, which is observed at ambient pressure in  $\text{BaVSe}_3$ . The decrease in  $\rho_0$  under pressure in  $\text{BaVSe}_3$  presumably comes from the fact that pressure modifies the interaction of magnetic moments and thus influences the scattering of conduction electrons on spin waves.

Contrary to pressure, applied magnetic field enhances  $\rho_0$ , approximately following  $\rho_0 \propto B^2$ . When an external magnetic field is present, in  $k$  space it separates the Fermi spheres of the spin-majority and spin-minority channels by  $\mu_B B$ . The field can change the configuration of the  $E_g$  electrons. The matrix element describing the transition from one spin orientation to the other is proportional to  $B^2$ . When random spin flips occur, the electronic orbitals of  $E_g$  electrons are influenced too. Since the conduction electrons from the  $A_{1g}$  sector scatter on the  $E_g$  electrons, when  $E_g$  electrons are canted or their distribution among minority and majority channels is changed, this may affect the scattering. The fact that the transition probability between the two spin orientations is proportional to  $B^2$  may be related to the similar field dependence of  $\rho_0$ .

## VII. DISCUSSION AND CONCLUSIONS

There is a considerable similarity between the high-pressure  $\text{BaVS}_3$  and the ambient-pressure  $\text{BaVSe}_3$ . When sulfur is replaced by selenium, the overlaps between the chains are enhanced, producing as an effect the chemical pressure. The aftermath is that there exists a set of physical properties which behave in a very similar manner. This is particularly clear in the case of the transport coefficients. The ambient-pressure-temperature dependence of the resistivity in  $\text{BaVSe}_3$  has the same qualitative shape as the resistivity in the sulfide for  $p > p_{cr}$  and the same holds for the thermoelectric power. What is more, the low-temperature resistivity in

the selenide is described by the canonical Fermi-liquid exponent  $n=2$ .

Experimenting on  $\text{BaVSe}_3$  allows an insight into the high-pressure phase of  $\text{BaVS}_3$ , warranting the use of many techniques which are normally inaccessible other than at ambient pressure. The measurements on  $\text{BaVSe}_3$ , besides confirming what we already know about  $\text{BaVS}_3$ , have also given some useful hints for understanding the magnetic ground state of the sulfide compound. The magnetic susceptibility infers that below 43 K,  $\text{BaVSe}_3$  is ferromagnetic. The ferromagnetic metallicity of the sister selenide suggests that the high-pressure ground state of  $\text{BaVS}_3$  is also likely to be ferromagnetic. However, the magnetic ground state of high-pressure  $\text{BaVS}_3$  is not yet experimentally accessible. From the high-temperature behavior of the resistivity and thermoelectric power of  $\text{BaVSe}_3$ , one is enticed to believe that the high-temperature phase of  $\text{BaVS}_3$  is also a bad metal characterized by linear temperature dependencies of the resistivity and the thermoelectric power.

In view of the band-structure calculations, it seems that it is not crucial to take into account the strong correlations in order to reproduce the main experimental observations that  $\text{BaVSe}_3$  is a ferromagnetic system of itinerant electrons. Band-structure calculations give a fairly correct estimate of the magnetic moment in the ferromagnetic phase. In addition, they predict that the bandwidths are not significantly influenced by our experimentally attainable pressures.

The correlation between the magnetic torque and the susceptibility allowed to see that the symmetry seen by the magnetic ions is changing below 200 K.<sup>5</sup> Moreover, the temperature dependence of the susceptibility anisotropy implies that below 62 K the system becomes most paramagnetic along the  $c$  axis, suggesting that a rotation of the magnetic axes takes place at this temperature. Consequently, there may be a structural transition happening at low temperatures or alternatively a deformation of the ligand cage. The resistivity departs from the linear temperature dependence and starts decreasing more steeply below 200 K. Again, this finding may also prove to be relevant for the high-pressure  $\text{BaVS}_3$ , in which the resistivity above  $p_{cr}$  has a very similar shape to that of  $\text{BaVSe}_3$ ; in that it also exhibits a change in slope around 200 K and a precipitous decrease below.<sup>8,11</sup>

Lastly, some of our observations induced us to believe that there is more complexity to the phenomena occurring in  $\text{BaVSe}_3$  than just what seems to be the continuation of high-pressure phase diagram of  $\text{BaVS}_3$ . One of the initial motives in the study of  $\text{BaVSe}_3$  was a possibility of stabilizing a non-Fermi-liquid state by pressure, just as it happens in the case of  $\text{MnSi}$ . There, the ferromagnetic transition is suppressed for pressures beyond 1.5 GPa, and the non-Fermi-liquid phase suddenly sets in as the power-law exponent jumps from  $n=2$  to  $3/2$ .<sup>28</sup> In  $\text{BaVSe}_3$ , we have not observed such a sudden drop in  $n$ . Instead, the power-law exponent  $n$  shows a decided increase under pressure. The residual resistivity  $\rho_0$  is dependent on pressure and magnetic field. Presently, we attribute these unexpected dependencies to the strong interaction between the  $E_g$  and the  $A_{1g}$  electrons.

## ACKNOWLEDGMENTS

The experimental work in Lausanne was sponsored by the

Swiss National Science Foundation and its NCCR MaNEP. Calculations were performed at the Computer Center of the Ecole Polytechnique Fédérale de Lausanne and at the Swiss Center for Scientific Computing in Manno. A part of this work was supported by the Swiss National Science Founda-

tion under Grant No. 200020-112318. The work in Zagreb was supported by the resources of the SNSF-SCOPES project (Scientific Cooperation between Eastern Europe and Switzerland) and by the Croatian Ministry of Science, Education and Sports under Grant No. 035-0352843-2846.

\*ana.akrap@epfl.ch

- <sup>1</sup>Y. Tokura, Rep. Prog. Phys. **69**, 797 (2006).
- <sup>2</sup>C. Pfleiderer, S. R. Julian, and G. G. Lonzarich, Nature (London) **414**, 427 (2001).
- <sup>3</sup>C. Pfleiderer, D. Reznik, L. Pintschovius, H. von Löhneysen, M. Garst, and A. Rosch, Nature (London) **427**, 227 (2004).
- <sup>4</sup>T. Yamasaki, S. Giri, H. Nakamura, and M. Shiga, J. Phys. Soc. Jpn. **70**, 1768 (2001).
- <sup>5</sup>M. Herak, M. Miljak, A. Akrap, L. Forró, and H. Berger, J. Phys. Soc. Jpn. **77**, 093701 (2008).
- <sup>6</sup>G. Mihaly, I. Kezsmarki, F. Zamborszky, M. Miljak, K. Penc, P. Fazekas, H. Berger, and L. Forro, Phys. Rev. B **61**, R7831 (2000).
- <sup>7</sup>H. Nakamura, T. Yamasaki, S. Giri, H. Imai, M. Shiga, K. Kojima, M. Nishi, K. Kakurai, and N. Metoki, J. Phys. Soc. Jpn. **69**, 2763 (2000).
- <sup>8</sup>L. Forró, R. Gaál, H. Berger, P. Fazekas, K. Penc, I. Kézsmárki, and G. Mihály, Phys. Rev. Lett. **85**, 1938 (2000).
- <sup>9</sup>J. Kelber, A. H. Reis, A. T. Aldred, M. H. Mueller, O. Massenet, G. Depasquali, and G. Stucky, J. Solid State Chem. **30**, 357 (1979).
- <sup>10</sup>N. Barišić, A. Akrap, H. Berger, and L. Forró, arXiv:0712.3395 (unpublished).
- <sup>11</sup>N. Barišić, A. Akrap, H. Berger, and L. Forró, arXiv:0712.3393 (unpublished).
- <sup>12</sup>J. P. Perdew, K. Burke, and M. Ernzerhof, Phys. Rev. Lett. **77**, 3865 (1996).
- <sup>13</sup>P. Giannozzi, <http://www.quantum-espresso.org>
- <sup>14</sup>H. J. Monkhorst and J. D. Pack, Phys. Rev. B **13**, 5188 (1976).
- <sup>15</sup>C.-L. Fu and K.-M. Ho, Phys. Rev. B **28**, 5480 (1983).
- <sup>16</sup>M. Parrinello and A. Rahman, Phys. Rev. Lett. **45**, 1196 (1980).
- <sup>17</sup>A. Akrap, A. Rudolf, F. Rullier-Albenque, H. Berger, and L. Forró, Phys. Rev. B **77**, 115142 (2008).
- <sup>18</sup>N. Barišić, Ph. D. thesis, Lausanne, 2004, <https://nanotubes.epfl.ch/nbarisic>
- <sup>19</sup>R. D. Barnard, *Thermoelectricity in Metals and Alloys* (Taylor & Francis, London, 1972).
- <sup>20</sup>Note that platinum, a conventional metal, has also a large intercept of thermoelectric power at  $T=0$  K, whose origin has never been elucidated. See, for example, J.-S. Zhou and J. B. Goodenough, Phys. Rev. B **51**, 3104 (1995).
- <sup>21</sup>P. Balla and P. Fazekas (unpublished).
- <sup>22</sup>N. J. Poulsen, Mater. Res. Bull. **32**, 1673 (1997).
- <sup>23</sup>In the hexagonal phase  $b=a\sqrt{3}=12.14$  Å.
- <sup>24</sup>The local symmetry of the vanadium atoms coincides with the point group of the BaVSe<sub>3</sub> in the hexagonal phase. Therefore the same labeling is used for the atomic orbitals and electronic states in the bulk at the  $\Gamma$  point.
- <sup>25</sup>M. Damnjanovic, T. Vukovic, and I. Milosevic, J. Phys. A **33**, 6561 (2000).
- <sup>26</sup>F. Lechermann, S. Biermann, and A. Georges, Phys. Rev. B **76**, 085101 (2007).
- <sup>27</sup>F. Lechermann, S. Biermann, and A. Georges, Phys. Rev. Lett. **94**, 166402 (2005).
- <sup>28</sup>C. Pfleiderer, G. J. McMullan, S. R. Julian, and G. G. Lonzarich, Phys. Rev. B **55**, 8330 (1997).
- <sup>29</sup>H. Nakamura and T. Kobayashi (unpublished).
- <sup>30</sup>A. Gauzzi, N. Barišić, F. Licci, G. Calestani, F. Bolzoni, P. Fazekas, E. Gilioli, and L. Forró, arXiv:cond-mat/0601286 (unpublished).
- <sup>31</sup>P. B. Allen (private communication).
- <sup>32</sup>N. F. Mott, Proc. Phys. Soc. London **47**, 571 (1935).
- <sup>33</sup>J. Mathon, Proc. R. Soc. London, Ser. A **306**, 355 (1968).
- <sup>34</sup>A. Ishikawa, J. Phys. Soc. Jpn. **51**, 441 (1982).